Monoenergetic High-Energy Ion Source via Femtosecond Laser Interacting with a Microtape

X. F. Shen [1] A. Pukhov [1,*] and B. Qiao [2,†]

[1]*Institut für Theoretische Physik I, Heinrich-Heine-Universität Düsseldorf, 40225 Düsseldorf, Germany*
[2]*Center for Applied Physics and Technology, HEDPS, SKLNP, and School of Physics,*
Peking University, Beijing, 100871, China

Intense laser-plasma ion sources are characterized by an unsurpassed acceleration gradient and exceptional beam emittance. They are promising candidates for next-generation accelerators towards a broad range of potential applications. However, the laser-accelerated ion beams available currently have limitations in energy spread and peak energy. Here, we propose and demonstrate an all-optical single laser scheme to generate proton beams with low spread at about 1% level and hundred MeV energy by irradiating the edge of a microtape with a readily available femtosecond petawatt laser. Three-dimensional particle-in-cell simulations show that when the electron beam extracted from both sides of the tape is injected into vacuum, a longitudinal bunching and transverse focusing field is self-established because of its huge charge (about 100 nC) and small divergence. Protons are accelerated and bunched simultaneously, leading to a monoenergetic high-energy proton beam. The proposed scheme opens a new route for the development of future compact ion sources.

I. INTRODUCTION

The development of compact laser-plasma ion sources has attracted significant attention in the past two decades [1–5]. Prospective applications include production of warm dense matter [6,7], proton radiography for implosion dynamics and ultrafast science [8,9], nuclear physics [10], tumor therapy [11], etc. For many of these applications, quasimonoenergetic ion beams are preferred [6,11,12], especially for tumor therapy, which requires energy spread of only about 1% [2,3,11]. An energy-selection system out of a broad energy spectrum ion source would sophisticate the device and lead to huge particle losses [7,13]. Because of the advancements in both laser technology and targetry, several breakthroughs have been successfully achieved in recent laser-ion acceleration experiments [14–16]. Proton beams with cutoff energy near 100 MeV [15,16] and carbon ions of about 50 MeV/μ [17] have been demonstrated in various laser systems. However, they still exhibit exponentially decaying energy spectra. Meanwhile, most of the experiments that established new records of maximum proton energy at their

publication time were accomplished on large laser facilities that deliver 100s J energy within a picosecond at low-repetition rate [1,14,16,18]. These lasers can be operated only in a few national laboratories [19,20]. In comparison, a high-repetition rate, low-cost, stable femtosecond laser is more preferable for developing the future compact ion sources. Actually, 100 Terawatt (TW)-class femtosecond laser systems have been widely distributed, and many multi-petawatt (PW) systems are currently operational, under construction, or in the planning phase [19], for which the generation of monoenergetic high-energy ion beams is one of the primary applications.

To achieve monoenergetic ion beams, a longitudinal bunching accelerating field is important, in which fast ions experience a smaller field and the slow ones a larger field. In traditional radio-frequency accelerators, such a bunching field is realized by controlling the phase of the synchronous particle relative to the crest of the accelerating wave [21], while in laser-ion acceleration, it appears as a longitudinal, negative gradient electric field acting on the accelerated ions. In one of the most-investigated laser-ion acceleration mechanisms—radiation pressure acceleration (RPA) [22–28]—such a bunching field was supposed to exist by piling excessive electrons at the rear surface. However, the RPA is plagued by strong electron heating due to effects of transverse instabilities [29,30] and finite spot size [31]. These effects may induce relativistic transparency and destroy the bunching electric field. As a consequence, the obtained ion energy is rather limited, and energy spread is very large. To obtain monoenergetic ion beams, the RPA

*[*]pukhov@tp1.uni-duesseldorf.de
[†]bqiao@pku.edu.cn

requires ultrahigh intensity, ultrahigh contrast, and a large spot size simultaneously, which remains a big challenge in experiments, even for multi-PW lasers [19].

In the other widely studied mechanism—target normal sheath acceleration (TNSA) [32–36]—this longitudinal bunching field is absent because of the low density of energetic electrons. The energy spectrum of TNSA ions is characterized by an exponential decay. Moreover, the maximum proton energy is related to the laser pulse energy, under other similar conditions, which usually means much lower ion energies for short femtosecond laser pulses [37–39].

Significant efforts have been devoted to overcoming the limitations of these mechanisms to improve the ion beam parameters, especially the energy spread and maximum energy. Here, we mention target designs [34,40–45], multi-pulse schemes [46–48], post-acceleration [49], and novel mechanisms [50–54]. Nevertheless, the obtained energy spreads are still larger than 10% because of the absence of a self-established bunching field. Therefore, in both theory and experiment, how to produce high-energy (like 100-MeV protons), monoenergetic (energy spread of about 1%) ion beams is still an open question.

In this paper, we propose a scheme named peeler acceleration, where a longitudinal bunching accelerating field builds up spontaneously when a currently available femtosecond laser pulse is incident on the edge of a simple microscale plasma tape, as shown by Fig. 1. As the laser pulse sweeps along the tape, it peels off abundant buckets of electrons from the tape into vacuum. These electrons are mainly accelerated forward along the tape surface to
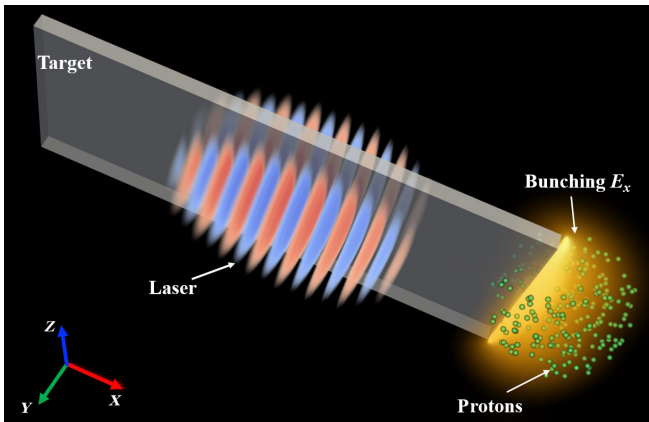

FIG. 1. Schematics of our peeler scheme. A femtosecond laser (red and blue) is incident on the edge of a microscale tape (grey). The micron-thick tape is infinitely long across the laser focus and is a few tens of microns wide along the laser propagation direction. Abundant electrons are continuously dragged out and accelerated forward by the intense laser. When these energetic electrons arrive at the rear edge of the tape, a longitudinal bunching field is established (yellow). Protons (green dots) are simultaneously accelerated and bunched by this field, leading to a highly monoenergetic proton beam.

superponderomotive energies by the longitudinal field of a surface plasma wave (SPW) [55–57]. The charge of energetic electrons (many tens to hundreds of nC) injected into the accelerating region at the rear edge of the tape is much larger than that of protons placed there (just a few nC), which ensures that the protons near the laser propagation axis are surrounded by the excessive space charge of electrons. This electron charge excess results in a negative gradient, longitudinal bunching field and a transverse focusing field simultaneously. Finally, a quasimonoenergetic proton beam with a peak energy of more than 100 MeV, energy spread of about 1%, and particle number of about 10^9 can be stably obtained with a laser pulse characterized by intensity greater than 10^{20} W/cm^2, pulse duration of about 45 fs, and energy of about 50 J.

II. MODEL AND SIMULATION PARAMETERS

Figure 1 illustrates the proposed peeler scheme, where an intense y-polarized laser pulse is incident on an edge of a microscale tape. The microtape can be infinitely long along the z direction, and laser pulses at grazing incidence are also applicable. The three-dimensional (3D) particle-in-cell (PIC) simulations are conducted with the EPOCH code [58] and the VLPL code [59]. The simulation box is $120\lambda \times 40\lambda \times 52.5\lambda$ in the $x \times y \times z$ directions, containing $2400 \times 1600 \times 1050$ cells, respectively. Here, a higher resolution in the y direction is used to resolve the plasma skin depth and the process of extracting electrons from the tape since a y-polarized laser pulse is chosen. We use a larger box length in the z direction because of a large tape to avoid the effects caused by the transverse recirculation of energetic electrons and mimic the real experimental situation.

The laser intensity is $I_0 = 7.8 \times 10^{20}$ W/cm^2 ($a_0 = 19$), with wavelength $\lambda = 800$ nm. The laser pulse has a Gaussian profile in both space and time, with radius $r_L = 7.5\lambda$ and pulse duration $\tau_L = 45$ fs, respectively, which is focused at the front edge of the tape. A plasma tape of high-Z material (we assume gold) has dimensions $x \times y \times z = 43.75\lambda \times 0.75\lambda \times 45\lambda$. Its rear edge has been covered with a hydrocarbon (CH) layer to simulate possible contaminants existing in experiment. To reduce the computational resources, the electron densities for the plasma tape and CH layer are both chosen as relativistically overdense, $n_e = 30n_c$, where $n_c = \pi m_e c^2/e^2\lambda^2$ is the critical density. The initial charge states of ions are given according to the Ammosov-Delone-Krainov formula [60,61], which means the ion species are Au^{51+} in the main target, and C^{6+} and H$^+$ in the hydrocarbon layer. The transverse dimensions of the CH layer are $0.75\lambda \times 45\lambda$ (same as the tape), while the longitudinal one is set to 0.4λ to ensure a sufficiently large proton areal density for mimicking the components of the contaminants. The density ratio of proton to carbon ions is $n_p : n_{C^{6+}} = 1:1$. The macroparticles in each cell for electrons, gold ions,

carbon ions, and protons are 8, 1, 8, and 32, respectively. In the simulations for comparison, except for the ones given in the text, the parameters remain unchanged. Open boundary conditions for fields and particles are employed. The numerical convergence has been confirmed by comparing the interested physical quantities with simulations at different resolutions and with the two codes.

III. RESULTS

A. Generation of high-energy collimated electrons

When a laser pulse is incident along an overdense plasma surface with a sharp edge, a SPW can be easily excited and propagate at the plasma-vacuum interface (along the x direction) [55–57]. This is different from the case where the laser pulse is incident on the target plane at a finite angle, when corrugated surfaces and very special resonance conditions would be required for an efficient SPW excitation [62–65].

Let us consider that a SPW propagates along the interface between vacuum and a "cold" plasma. The longitudinal electric field on the vacuum side has the form [56]

$$E_{sw} = E_{sw0}e^{-k_y y}e^{-i(\omega t - k_x x)}, \qquad (1)$$

where E_{sw0} is the amplitude of the longitudinal SPW field, $k_y^2 = (k_x^2 - \omega^2/c^2)$, $k_x^2 = (\omega^2/c^2)(\epsilon/1 + \epsilon)$, $\epsilon = 1 - \omega_{pe}^2/\omega^2$ is the dielectric constant of the plasma, and $\omega_{pe} = \sqrt{4\pi n_e e^2/m_e}$ is the plasma frequency. For overdense plasma ($\omega_{pe} > \sqrt{2}\omega$), k_y is a real number, which indicates that the wave decays out from the surface. If $\omega_{pe} \gg \omega$, the phase velocity of the SPW is approximated to be $v_{ph}^{SPW} = \omega/k_x \approx c(1 - \omega^2/2\omega_{pe}^2)$, which is very close to the speed of light c. For a focused Gaussian laser pulse in vacuum, its phase velocity near the axis is determined by $v_{ph}^L = -(\partial\varphi/\partial t)/(\partial\varphi/\partial x)$, where φ is the total phase of the laser pulse [66]. For $x \ll z_R$, we have $v_{ph}^L \approx c(1 + \lambda^2/2\pi^2 w_0^2)$, which is slightly larger than c. Here, $z_R = \pi w_0^2/\lambda$ is the Rayleigh length, and $w_0 = 2r_L/\sqrt{2\ln(2)}$ is the waist radius. So the laser pulse and the SPW stay in phase over the dephasing distance L_d until the phase difference between both becomes $\Delta\phi = k_0 L_d \Delta v/c = \pi$, where $\Delta v = v_{ph}^L - v_{ph}^{SPW}$. Then, we get the dephasing length

$$L_d \simeq \lambda \frac{1}{\lambda^2/\pi^2 w_0^2 + \omega^2/\omega_{pe}^2}, \qquad (2)$$

indicating that the acceleration distance L_d can be much larger than the laser focal spot size. Further, the maximum electron energy is determined from $\epsilon_{e,\max} = \int eE_{sw}cdt$, yielding

$$\epsilon_{e,\max} \simeq \frac{2}{\pi}eE_{sw0}L_d. \qquad (3)$$

When the laser pulse reaches the rear side of the tape, assuming all the electrons within the skin depth on the two lateral surfaces are peeled off and accelerated to high energies, the number of energetic electrons can be estimated from a phenomenological model as

$$N_e \simeq 4r_L l_x l_s n_e, \qquad (4)$$

where l_x is the longitudinal width of the tape and $l_s = c/\omega_{pe}$ is the skin depth.

The 3D PIC simulation results are shown in Fig. 2. The longitudinal electric field E_{sw} of this SPW at $t = 22T_0$ is shown in Fig. 2(a), which reaches about $E_{sw0} \simeq 2.0 \times 10^{13}$ V/m and decays along the transverse direction. Here, $t = 0$ represents the time when the pulse peak enters the simulation box. Compared with the distribution of the laser field E_y in Fig. 2(c), one can see that the SPW travels with the laser pulse at velocities close to c, enabling an efficient laser-SPW coupling over a long distance. Figures 2(b) and 3(a) present the electron density distribution in the 2D and 3D perspective views, respectively. It is clearly shown that the high-density ($> 2.5n_c$) electron bunches are periodically distributed and separated by one laser wavelength on each side. Further, compared with Fig. 2(a), one can find that most of the electrons are trapped in the longitudinal potential well and accelerated by the negative component of the strong SPW field, resulting in a highly collimated electron beam with $p_x \gg p_\perp \gg m_e c$ [55]. Figure 2(d) shows the distribution of the quasistatic magnetic field B_z, which is induced by the large return current inside the tape, and its strength exceeds 1 GG.

Figure 4(a) presents the energy-gain plane of each electron at $t = 48T_0$, where the color scale represents the net electron energy. The energy gain is defined as

$$\Gamma_x = -\int_0^t ev_x E_x dt, \qquad (5)$$

$$\Gamma_y = -\int_0^t ev_y E_y dt. \qquad (6)$$

The black dashed lines enclose areas preferably populated by the longitudinal and transverse acceleration [67,68], respectively. For the highest-energy part, the longitudinal acceleration (SPW) always dominates. The evolution of the electron energy spectrum is shown in Fig. 4(b). One can see that more and more electrons are accelerated to higher energies. Both the effective temperature and maximum energy of the electron beam increase with time. When the electron beam reaches the rear edge of the tape ($t = 48T_0$), the effective temperature T_{eff} is about 36 MeV (red line), much larger than the value of 6.4 MeV given by
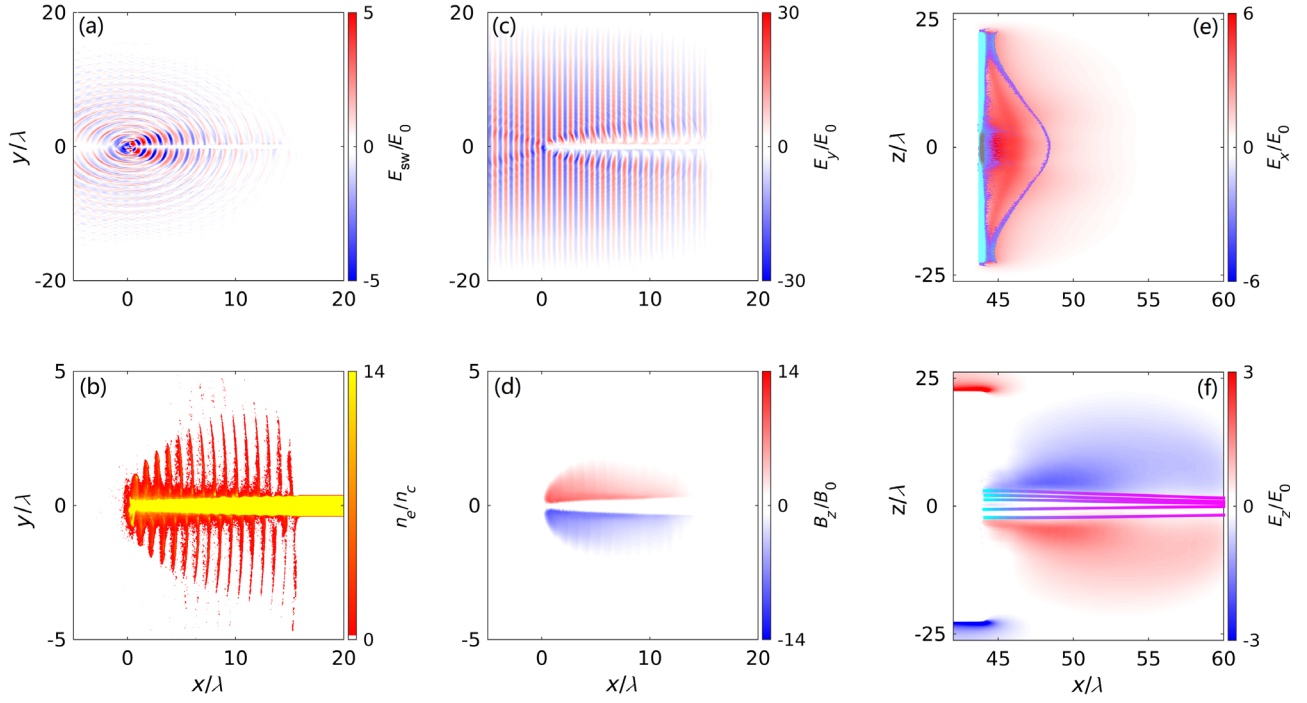
FIG. 2. Three-dimensional PIC simulation results. Distributions of the longitudinal electric field E_{sw} (a), electron density n_e (b), laser electric field E_y (c), and self-generated magnetic field B_z (d) at $t = 22T_0$ in the plane (x, y). Panels (e) and (f) show the averaged longitudinal electric field E_x and transverse electric field E_z at $t = 70T_0$ in the plane (x, z), respectively. In panel (e), the purple sheet represents the compressed proton layer, which is situated at the negative gradient region of E_x. In panel (f), the colored lines correspond to the collimated trajectories of selected protons, where the color represents the relative proton energy.

ponderomotive scaling $T_{pond} = (\sqrt{1 + a_0^2/2} - 1)m_e c^2$ [69]. The maximum electron energy reaches up to about 260 MeV at $t = 58T_0$.

According to Eq. (3), the maximum energy is predicted to be about 300 MeV by substituting the values of $E_{sw0} = 2 \times 10^{12}$ V/m and $\omega_{pe}^2/\omega^2 = 30$, which is in fair agreement with the simulation results, considering the simplicity of the model. Meanwhile, in the simulation, we observe that the charge of high-energy electrons ($\gamma_e > 10$) outside of the tape reaches about 128 nC ($\sim 10^{12}$), which is also in broad

accordance with the estimation of Eq. (4). Note that, here, the maximum electron energy is much higher than the model described in Ref. [62] since, in our scheme, the longitudinal acceleration dominates [see Fig. 4(a)] and the acceleration region is no longer limited by the focal spot size. The latter also significantly increases the number of energetic electrons.

B. Process of proton acceleration

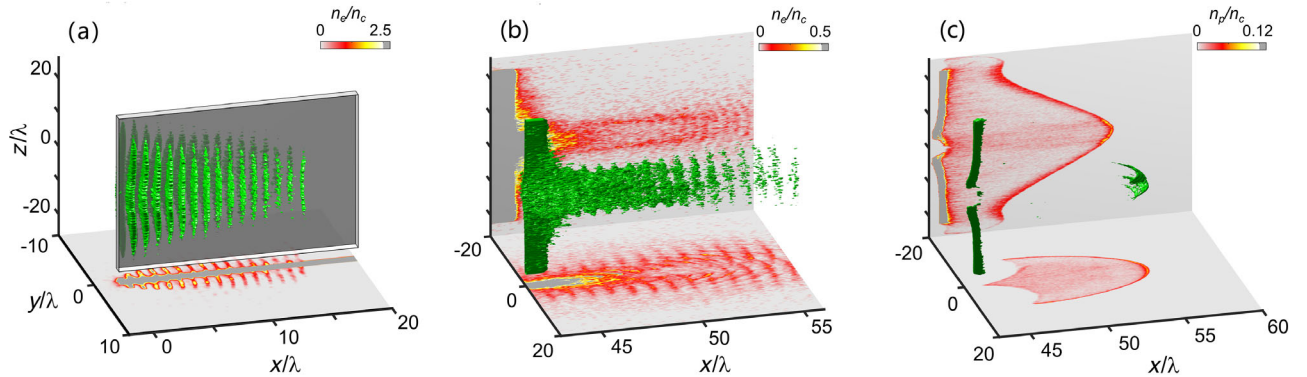When this collimated superponderomotive electron beam reaches the rear edge and exits into the vacuum

FIG. 3. Particle density distribution. (a,b) Electron density distributions at $t = 22T_0$ and $70T_0$, respectively. (c) Proton density distribution at $t = 86T_0$. The isosurface values in panels (a)–(c) are $n_e = 0.75n_c$, $n_e = 0.2n_c$, and $n_p = 0.07n_c$, respectively; the (x, y) projections are at $z = 0$ and the (x, z) projections at $y = 0$, except that in panel (a), only the (x, y) projection is shown.
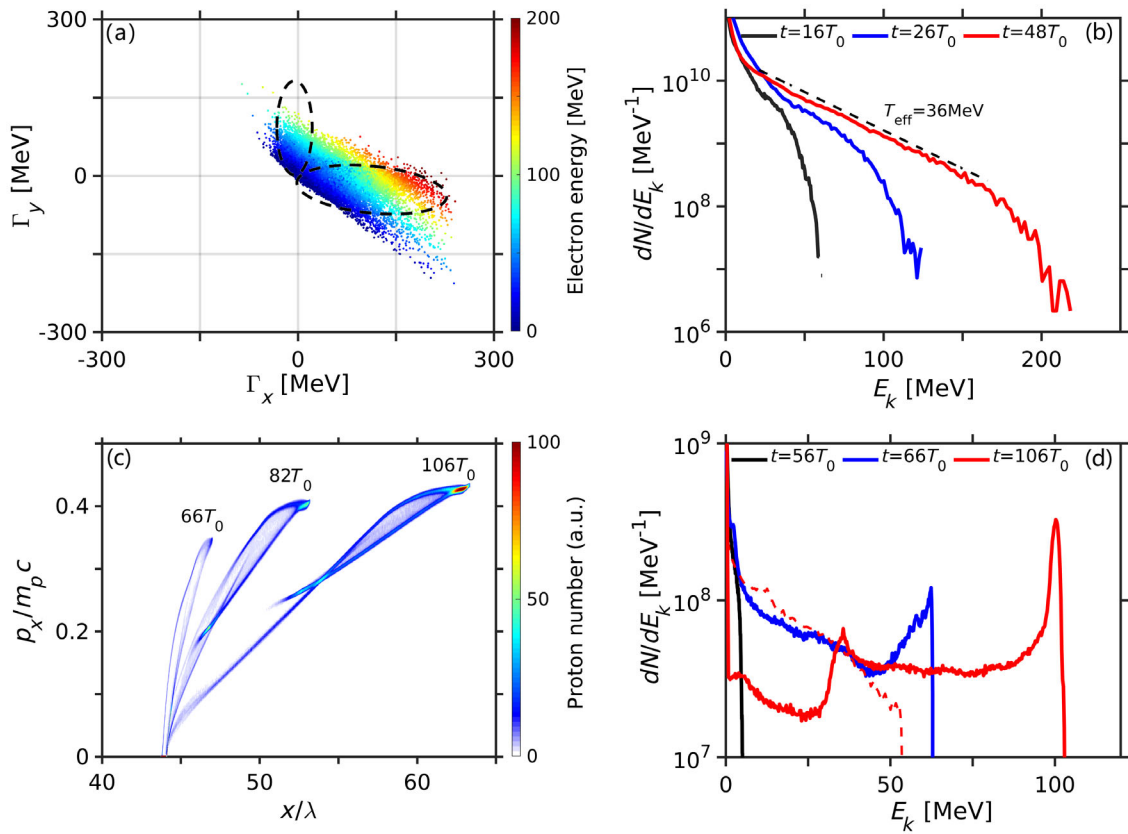
FIG. 4. Energy gain of electrons and evolution of particle energy spectrum. (a) Energy gain of electrons from the longitudinal (Γ_x) and transverse (Γ_y) directions, defined by Eqs. (5) and (6), respectively. The color scale represents the final electron energy. (b) Energy spectrum of electrons at $t = 16T_0$, $26T_0$, and $48T_0$. (c) Proton phase space at $t = 66T_0$, $82T_0$, and $106T_0$. (d) Black, blue, and red solid lines represent the energy spectrum of protons at $t = 56T_0$, $66T_0$, and $106T_0$, respectively. The red dashed line shows the energy spectrum of carbon ions at $t = 106T_0$.

[Fig. 3(b)], a high electron density, about $n_h = 2.5n_c$, is formed in vacuum near the tape edge. A strong longitudinal electrostatic field is established here [Fig. 2(e)]. The initial longitudinal field can be estimated as $E_{sh} = \sqrt{8\pi n_h T_{\mathrm{eff}}}/e_{\mathrm{N}} = 4.5 \times 10^{13}$ V/m, with $e_{\mathrm{N}} \approx 2.71828$ [37,70], which is consistent with the simulation result 5.0×10^{13} V/m and almost comparable to the peak value of the laser field.

This strong E_x pulls protons out of the CH layer and then accelerates them forward. The initial energy spectrum is broad, shown by the black line in Fig. 4(d). However, in peeler acceleration, the space charge of electrons injected into the vacuum can reach about 50 nC, which is much larger than the charge of protons (about 2.7 nC within the focus spot). As a consequence, protons, especially those around the propagation axis, are surrounded by a negative electron cloud. In one-dimensional situations, $\partial E_x/\partial x = -4\pi e(n_e - n_p)$. Therefore, protons are accelerated by a bunching field, as shown by the purple sheet in Fig. 2(e). This field structure is very similar to that in the "compressed electron layer" in RPA [71,72]. This bunching field compresses the proton phase space [Fig. 4(c)] and reduces

the energy spread [Fig. 4(d)] repeatedly. The highest energy part of the protons forms a distinct density peak ($\sim 0.1n_c$), as shown in Fig. 3(c). We should mention here that, different from the RPA, our scheme is free of the transverse instabilities.

From the evolution of the proton phase space in Fig. 4(c) and energy spectrum in Fig. 4(d), we observe that the bunching process lasts for more than 150 fs, which is about 4 times longer than the laser pulse duration τ_L. The reason for this is that the high-energy electrons have large recirculation radii and a small angular spread, so the electron recirculation is predominantly along the x direction. Both the forward- and backward-moving electrons help maintain the bunching field in a large region [more than 20λ long, as shown in Fig. 4(c)]. The strong, long-lasting bunching field not only leads to a highly efficient acceleration, but it also helps reduce the proton energy spread to an extremely low level. This result also explains why almost all the protons near the x axis are evacuated in Fig. 3(c), even that the thickness of the CH layer is already 0.4λ.

Another contribution of the collimated electron beam is that a transverse charge separation field E_z is induced, as shown by Fig. 2(f). Since there are excessive electrons in

the center, E_z provides a focusing force for protons. We show trajectories of some selected protons in Fig. 2(f), where the color marks the evolution of proton energy. One can clearly see that protons are focused by the field E_z, leading to more protons gather around the x axis, as shown by the (x, z) projection plane in Fig. 3(c). Such a self-established longitudinal bunching and transverse focusing field configuration makes our scheme robust and suitable for generation of monoenergetic ion beams, which is the key difference from the typical TNSA, where a debunching field dominates the acceleration process since the electron beam is characterized by the relatively small electron number and large angular spread [3,38]. In particular, the latter causes the hot electron density to decrease quickly during the propagation. Furthermore, compared to the requirement of a fragile balance condition in RPA [27,29], the bunching field in our peeler scheme is self-established on the basis of a large number of high-energy electrons, which is very robust as long as the tape is wide enough to provide the sufficient charge of electrons. Note that, though for electrons the field E_z provides a defocusing force, the strong self-generated angular magnetic field induced by the return current confines the electron beam, maintaining its collimation, as shown by the (x, z) plane projection in Fig. 3(b).

Figure 4(d) shows the energy spectrum of the proton beam at different times. At the beginning, the energy spread is large (black line) since protons feel a positive gradient E_x as they are pulled out from the CH layer. Subsequently, the energy spread decreases constantly because of the longitudinal bunching field caused by excessive electrons, as shown by the blue and red solid lines. Finally, for a high-energy quasimonoenergetic proton beam, with peak energy greater than 100 MeV, energy spread of about 1.2% is obtained (red line). The particle number within the peak (FWHM) reaches 8×10^8 (1.5×10^8) inside an angle of 10° (3°). The peak spectral brightness of the proton beam reaches 1.3×10^{10} protons/MeV/Sr in the forward direction, which is 1 order of magnitude higher than that of TNSA and RPA at the (much lower) cutoff energy [as the solid lines show in Fig. 6(c)]. The low-energy spread persists for a long time since the further contribution of Coulomb explosion could be ignored, considering the copropagating, collimated electron beam.

C. Scaling law study

Figure 5 illustrates the peak proton energy ϵ_p (black asterisks) and energy spread (red triangles) as a function of laser intensity I_0 obtained from 3D simulations, where the other parameters remain almost the same. The numerical results suggest that in peeler acceleration, the scaling of ϵ_p satisfies

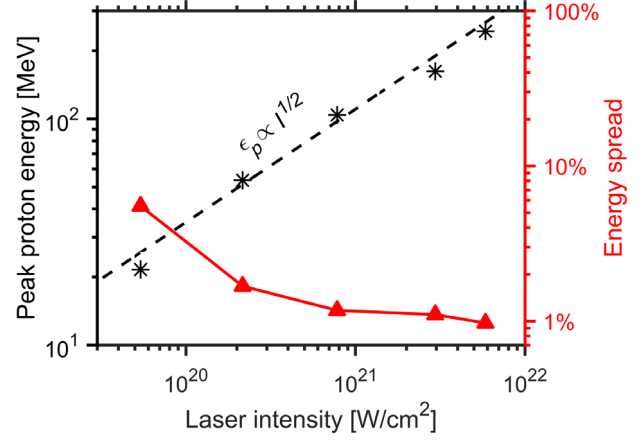$$\epsilon_p \sim \alpha (I_0/I_{18})^{1/2}, \qquad (7)$$

FIG. 5.   Peak proton energy ϵ_p (black asterisks) and energy spread (red triangles) with varying laser intensity, where the other parameters are kept almost the same as those of Fig. 2, except the electron density, to avoid the relativistic transparency. The dashed black line displays the best-fit scaling for peak proton energy.

with coefficients $\alpha \approx 3.5$ MeV and $I_{18} = 10^{18}$ W/cm². Though the scaling is similar to that of TNSA, the proportionality factor α is significantly higher, which stems from the high-quality electron beam characterized by large particle number, high effective temperature, and small divergence angle. More importantly, as the red triangles show in Fig. 5, the energy spread always stays at an extremely low level, and even with moderate intensity $I_0 < 10^{20}$ W/cm², it is still less than 10%. Proton beams with an energy spread at the 1% level can be stably obtained as the laser intensity increases, which is the key advantage of our scheme compared to the others. To the best of our knowledge, no experiments or 3D PIC simulations of laser-ion acceleration have reported such high-quality ion beams [2,3,5]. We mention that Ref. [73], where the experiments are performed with a CO_2 laser system, reports a proton beam with an energy spread of 1% but only about 10^5 protons within the peak.

IV. ROBUSTNESS OF THE SCHEME

Considering that in realistic experiments, there might be some fluctuations existing in the initial laser and plasma setups, we perform a series of 3D simulations to study the robustness of our scheme.

Figure 6(a) presents the final proton energy spectra obtained from the cases considering the changes of tape width l_x (black), thickness l_y (green), and the incidence angle θ_i (blue), where, except for the ones given in the legend, the parameters remain unchanged. One can see that a monoenergetic proton beam with energy spread at the 1% level and a peak energy of about 100 MeV can be robustly obtained. The detailed proton parameters can be found in the Table 1 of the Supplemental Material [74].
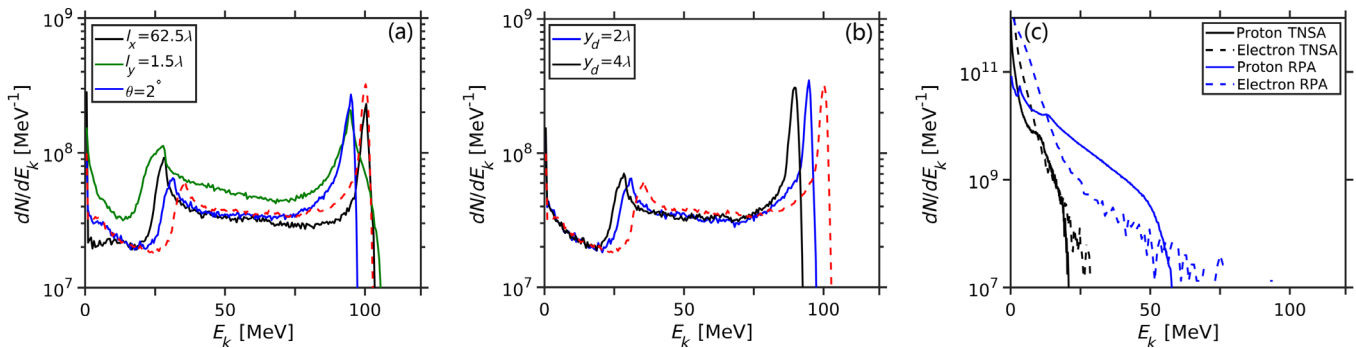
FIG. 6. Robustness study and comparison. (a) Proton energy spectra from the cases with different fluctuations considered, including the tape width l_x (black), thickness l_y (green), and the incidence angle θ_i (blue). (b) Proton energy spectra considering the effects of laser pointing stability. The blue and black solid lines represent the cases with misalignments of $y_d = 2\lambda$ and $y_d = 4\lambda$, respectively. In panels (a) and (b), the red dashed line represents the results from Fig. 4(d), for comparison. For each case displayed by the solid lines, except the difference given by the legend, the other parameters are the same as those described in the Figs. 2–4. (c) Electron (dashed lines) and proton (solid lines) energy spectra obtained from the TNSA (black) and RPA (blue) mechanisms with the same laser parameters.

Furthermore, to realize a stable particle beam source in experiment, the pointing stability of the laser is one of the most critical parameters, as it causes a misalignment between the laser focal spot center and the target center. This parameter has already aroused great concern in other experiments, such as laser-driven particle acceleration with structural (or mass-limited) targets [50,75,76] and collision of high-energy electrons with intense laser pulses [77,78]. In our scheme, the pointing stability may reduce the laser intensity on target, and therefore, the obtained proton energy would decrease following the scaling law of Eq. (7). According to the transverse profile of the laser pulse, one can easily estimate the attainable proton energy from the value of the misalignment. For example, using the laser parameters described in Sec. II, if the possible deviations along the y direction are $y_d = 0.27r_L$ (i.e., 2λ) and $0.54r_L$ (4λ), the obtained peak energies will be reduced to about 97 MeV and 90 MeV, respectively. They agree well with the 3D simulation results of about 95 MeV and 90 MeV, as shown by the blue and black lines, correspondingly, in Fig. 6(b). Therefore, we deduce that to ensure the energy fluctuation is less than 10% (20%), the laser spatial jitter should be smaller than $0.54r_L$ ($0.8r_L$). The requirement in the bracket is already within the state of the art [20,50,75–78], and much better performances can be expected in the near future [79]. It is worth mentioning that, to validate the key feature of this peeler scheme, i.e., monoenergetic proton energy spectra, the requirement on the laser pointing stability is not stringent. From Fig. 5, we can predict that even with a misalignment up to $2r_L$, a proton beam with an energy spread of less than 10% can still be obtained.

If the incidence angle is much larger than the divergence angle of the tightly focused Gaussian laser pulse such as 10°, our 3D simulations show that the peak energy is reduced to about 76 MeV while the energy spread stays extremely low. The simulation results and explanations can

be found in Fig. S1 and Note 2 of the Supplemental Material [74]. It is also noteworthy that in this geometry, the effects of the laser pointing stability are rather small. According to our 3D simulation results, even if the misalignment is as large as $0.85r_L$, the energy fluctuation is only about 3% because the peak intensity on target is almost the same, and electrons can obtain efficient acceleration via the longitudinal field of the SPW (incident on the front edge) or the superposition of incident and reflected fields (incident on the lateral surface at small angles) [80]. The details can be found in Fig. S2 and Note 2 of Supplemental Material [74].

We also conducted a 2D simulation with realistic electron density (about $2000n_c$) and preplasma composed of hydrocarbon (covered around the tape) considered; the main physical process and results remain the same (see Fig. S3 of the Supplemental Material [74]). Since protons originating from the lateral surfaces are mainly accelerated transversely, a highly monoenergetic forward proton beam can be obtained. Neither energy spread nor the peak energy of the proton beam is sensitive to the scale length of the preplasma, which demonstrates that our scheme can tolerate the existence of an appropriate level of preplasma.

V. DISCUSSION

In our simulations, the tape length was $l_z = 45\lambda$ (limited by the simulation box size), which is 6 times larger than the radius of the laser pulse. The time (about $45T_0$) for electrons recirculating from the boundary along the z direction is about 3 times longer than the pulse length (about $17T_0$). When the electrons recirculate back from the boundary, the high-energy protons are accelerated 10s λ forward. Only those with lower energies could benefit from this recirculation. Therefore, a further increase of the tape length does not change the main results, like the peak energy, energy spread, and proton number with the peak.

In other words, in experiment, a very long tape along the z direction can be used to validate our method. Targets with similar parameters can be fabricated with current targetry [81–83], and a possible approach to a high-repetition rate operation of our scheme is to mount the targets in each array of a target positioning system [82] (see details in Fig. S4 and Note 4 of the Supplemental Material [74]).

As a baseline comparison, we also performed 3D simulations with a laser pulse obliquely incident on a flat target with incidence angle 30°, where the laser parameters remained the same. The energy spectra of electrons and protons are shown by the dashed and solid black lines in Fig. 6(c), respectively. The effective temperature is much lower, and the energy spectrum is broad, with a cutoff energy about 5 times less than that in our scheme. Furthermore, the blue lines correspondingly show the results from a target with area density satisfying the optimal condition of RPA [72]. Because of the effects of instabilities [27,29,30], significant electron heating occurs, and the target is penetrated during the acceleration. Therefore, the electron temperature is even higher than that of TNSA [30]. The proton energy spectrum is exponentially decaying, and the maximum energy is only half of ours.

In recent experiments, Cristoforetti *et al.* observed enhancements of both the flux and the cutoff energy of protons by irradiating nanotube array targets with intense laser pulses, where the SPW is excited at the entrance of the tubes [84,85]. However, limited by the targetry, the diameter of the nanotube is not optimal for the laser-SPW coupling, and a thick substrate is necessary to hold the nanotubes. Therefore, protons are still accelerated via the standard TNSA, and the obtained energy spectrum is exponentially decaying.

VI. SUMMARY

In summary, we proposed a robust scheme for achieving high-energy proton beams with energy spread at the percent level, where a longitudinal bunching and transverse focusing field is self-established through irradiating a femtosecond laser pulse on an edge of a microscale tape. These results illustrate the potential of achieving monoenergetic high-energy ion beams in readily available femtosecond laser facilities without stringent requirements on the laser polarization and temporal pulse contrast. This novel interaction geometry also offers great opportunities for the studies of high-energy-density physics, particle, and radiation sources. For example, as the high-energy electrons move forward, a large return current, and therefore a strong quasistatic magnetic field, is induced, which could compress the plasma to an ultrahigh density [86,87] (see Fig. S3 of the Supplemental Material [74]). Therefore, we expect a microscale ultradense Z pinch to form. By substituting the target material with a deuterium-containing material, an ultrafast neutron beam can be efficiently generated.

[1] R. A. Snavely, M. H. Key, S. P. Hatchett, T. E. Cowan, M. Roth, T. W. Phillips, M. A. Stoyer, E. A. Henry, T. C. Sangster, M. S. Singh *et al.*, *Intense High-Energy Proton Beams from Petawatt-Laser Irradiation of Solids*, Phys. Rev. Lett. **85**, 2945 (2000).

[2] A. Macchi, M. Borghesi, and M. Passoni, *Ion Acceleration by Superintense Laser-Plasma Interaction*, Rev. Mod. Phys. **85**, 751 (2013).

[3] H. Daido, M. Nishiuchi, and A. S. Pirozhkov, *Review of Laser-Driven Ion Sources and Their Applications*, Rep. Prog. Phys. **75**, 056401 (2012).

[4] A. Macchi, *A Review of Laser-Plasma Ion Acceleration*, arXiv:1712.06443.

[5] B. Qiao, X. F. Shen, H. He, Y. Xie, H. Zhang, C. T. Zhou, S. P. Zhu, and X. T. He, *Revisit on Ion Acceleration Mechanisms in Solid Targets Driven by Intense Laser Pulses*, Plasma Phys. Controlled Fusion **61**, 014039 (2019).

[6] E. Brambrink, T. Schlege, G. Malka, K. U. Amthor, M. M. Aléonard, G. Claverie, M. Gerbaux, F. Gobet, F. Hannachi, V. Méot *et al.*, *Direct Evidence of Strongly Inhomogeneous Energy Deposition in Target Heating with Laser-Produced Ion Beams*, Phys. Rev. E **75**, 065401(R) (2007).

[7] M. Schollmeier, S. Becker, M. Geißel, K. A. Flippo, A. Blažević, S. A. Gaillard, D. C. Gautier, F. Grüner, K. Harres, M. Kimmel *et al.*, *Controlled Transport and Focusing of Laser-Accelerated Protons with Miniature Magnetic Devices*, Phys. Rev. Lett. **101**, 055004 (2008).

[8] M. Borghesi, A. Schiavi, D. H. Campbell, M. G. Haines, O. Willi, A. J. MacKinnon, L. A. Gizzi, M. Galimberti, R. J. Clarke, and H. Ruhl, *Proton Imaging: A Diagnostic for Inertial Confinement Fusion/Fast Ignitor Studies*, Plasma Phys. Controlled Fusion **43**, A267 (2001).

[9] C. K. Li, F. H. Séguin, J. A. Frenje, J. R. Rygg, R. D. Petrasso, R. P. J. Town, P. A. Amendt, S. P. Hatchett, O. L. Landen, A. J. Mackinnon, P. K. Patel *et al.*, *Measuring E and B Fields in Laser-Produced Plasmas with Mono-energetic Proton Radiography*, Phys. Rev. Lett. **97**, 135003 (2006).

[10] F. N. Beg, K. Krushelnick, C. Gower, S. Torn, A. E. Dangor, A. Howard, T. Sumner, A. Bewick, V. Lebedenko, J. Dawson *et al.*, *Table-Top Neutron Source for Characterization and Calibration of Dark Matter Detectors*, Appl. Phys. Lett. **80**, 3009 (2002).

[11] S. V. Bulanov, T. Z. Esirkepov, V. S. Khoroshkov, A. V. Kuznetsov, and F. Pegoraro, *Oncological Hadron Therapy with Laser Ion Accelerators*, Phys. Lett. A **299**, 240 (2002).

[12] B. M. Hegelich, D. Jung, B. J. Albright, J. C. Fernandez, D. C. Gautier, C. Huang, T. J. Kwan, S. Letzring, S. Palaniyappan, R. C. Shah *et al.*, *Experimental Demonstration of Particle Energy, Conversion Efficiency and Spectral Shape Required for Ion-Based Fast Ignition*, Nucl. Fusion **51**, 083011 (2011).

[13] U. Linz and J. Alonso, *Laser-Driven Ion Accelerators for Tumor Therapy Revisited*, Phys. Rev. Accel. Beams **19**, 124802 (2016).

[14] F. Wagner, O. Deppert, C. Brabetz, P. Fiala, A. Kleinschmidt, P. Poth, V. A. Schanz, A. Tebartz, B. Zielbauer, M. Roth *et al.*, *Maximum Proton Energy above 85 MeV from the Relativistic Interaction of Laser Pulses with Micrometer Thick CH_2 Targets*, Phys. Rev. Lett. **116**, 205002 (2016).

[15] I. J. Kim, K. H. Pae, I. W. Choi, C.-L. Lee, H. T. Kim, H. Singhal, J. H. Sung, S. K. Lee, H. W. Lee, P. V. Nickles *et al.*, *Radiation Pressure Acceleration of Protons to 93 MeV with Circularly Polarized Petawatt Laser Pulses*, Phys. Plasmas **23**, 070701 (2016).

[16] A. Higginson, R. J. Gray, M. King, R. J. Dance, S. D. R. Williamson, N. M. H. Butler, R. Wilson, R. Capdessus, C. Armstrong, J. S. Green *et al.*, *Near-100 MeV Protons via a Laser-Driven Transparency-Enhanced Hybrid Acceleration Scheme*, Nat. Commun. **9**, 724 (2018).

[17] W. J. Ma, I Jong Kim, J. Q. Yu, I. W. Choi, P. K. Singh, H. W. Lee, J. H. Sung, S. K. Lee, C. Lin, Q. Liao *et al.*, *Laser Acceleration of Highly Energetic Carbon Ions Using a Double-Layer Target Composed of Slightly Underdense Plasma and Ultrathin Foil*, Phys. Rev. Lett. **122**, 014803 (2019).

[18] S. A. Gaillard, T. Kluge, K. A. Flippo, M. Bussmann, B. Gall, T. Lockard, M. Geissel, D. T. Offermann, M. Schollmeier, Y. Sentoku *et al.*, *Increased Laser-Accelerated Proton Energies via Direct Laser-Light-Pressure Acceleration of Electrons in Microcone Targets*, Phys. Plasmas **18**, 056710 (2011).

[19] C. Danson, D. Hillier, N. Hopps, and D. Neely, *Petawatt Class Lasers Worldwide*, High Power Laser Sci. Eng. **3**, e3 (2015).

[20] C. Danson, C. Haefner, J. Bromage, T. Butcher, J.-C. F. Chanteloup, E. A. Chowdhury, A. Galvanauskas, L. A. Gizzi, J. Hein, D. I. Hillier *et al.*, *Petawatt and Exawatt Class Lasers Worldwide*, High Power Laser Sci. Eng. **7**, e54 (2019).

[21] T. P. Wangler, *Principles of RF Linear Accelerators* (John Wiley & Sons, New York, 1998), p. 172.

[22] T. Esirkepov, M. Borghesi, S. V. Bulanov, G. Mourou, and T. Tajima, *Highly Efficient Relativistic-Ion Generation in the Laser-Piston Regime*, Phys. Rev. Lett. **92**, 175003 (2004).

[23] A. P. L. Robinson, M. Zepf, S. Kar, R. G. Evans, and C. Bellei, *Radiation Pressure Acceleration of Thin Foils with Circularly Polarized Laser Pulses*, New J. Phys. **10**, 013021 (2008).

[24] B. Qiao, M. Zepf, M. Borghesi, and M. Geissler, *Stable GeV Ion-Beam Acceleration from Thin Foils by Circularly Polarized Laser Pulses*, Phys. Rev. Lett. **102**, 145002 (2009).

[25] B. Qiao, M. Zepf, M. Borghesi, B. Dromey, M. Geissler, A. Karmakar, and P. Gibbon, *Radiation-Pressure Acceleration of Ion Beams from Nanofoil Targets: The Leaky Light-Sail Regime*, Phys. Rev. Lett. **105**, 155002 (2010).

[26] A. Henig, S. Steinke, M. Schnürer, T. Sokollik, R. Hörlein, D. Kiefer, D. Jung, J. Schreiber, B. M. Hegelich, X. Q. Yan, J. Meyer-ter-Vehn *et al.*, *Radiation-Pressure Acceleration of Ion Beams Driven by Circularly Polarized Laser Pulses*, Phys. Rev. Lett. **103**, 245003 (2009).

[27] X. F. Shen, B. Qiao, H. Zhang, S. Kar, C. T. Zhou, H. X. Chang, M. Borghesi, and X. T. He, *Achieving Stable Radiation Pressure Acceleration of Heavy Ions via Successive Electron Replenishment from Ionization of a High-Z Material Coating*, Phys. Rev. Lett. **118**, 204802 (2017).

[28] C. Scullion, D. Doria, L. Romagnani, A. Sgattoni, K. Naughton, D. R. Symes, P. McKenna, A. Macchi, M. Zepf, S. Kar *et al.*, *Polarization Dependence of Bulk Ion Acceleration from Ultrathin Foils Irradiated by High-Intensity Ultrashort Laser Pulses*, Phys. Rev. Lett. **119**, 054801 (2017).

[29] F. Pegoraro and S. V. Bulanov, *Photon Bubbles and Ion Acceleration in a Plasma Dominated by the Radiation Pressure of an Electromagnetic Pulse*, Phys. Rev. Lett. **99**, 065002 (2007).

[30] Y. Wan, I. A. Andriyash, W. Lu, W. B. Mori, and V. Malka, *V. Effects of the Transverse Instability and Wave Breaking on the Laser-Driven Thin Foil Acceleration*, Phys. Rev. Lett. **125**, 104801 (2020).

[31] F. Dollar, C. Zulick, A. G. R. Thomas, V. Chvykov, J. Davis, G. Kalinchenko, T. Matsuoka, C. McGuffey, G. M. Petrov, L. Willingale *et al.*, *Finite Spot Effects on Radiation Pressure Acceleration from Intense High-Contrast Laser Interactions with Thin Targets*, Phys. Rev. Lett. **108**, 175005 (2012).

[32] A. Pukhov, *Three-Dimensional Simulations of Ion Acceleration from a Foil Irradiated by a Short-Pulse Laser*, Phys. Rev. Lett. **86**, 3562 (2001).

[33] S. C. Wilks, A. B. Langdon, T. E. Cowan, M. Roth, M. Singh, S. Hatchett, M. H. Key, D. Pennington, A. MacKinnon, and R. A. Snavely, *Energetic Proton Generation in Ultra-Intense Laser-Solid Interactions*, Phys. Plasmas **8**, 542 (2001).

[34] H. Schwoerer, S. Pfotenhauer, O. Jäckel, K.-U. Amthor, B. Liesfeld, W. Ziegler, R. Sauerbrey, K. W. D. Ledingham, and T. Esirkepov, *Laser-Plasma Acceleration of Quasi-Monoenergetic Protons from Microstructured Targets*, Nature (London) **439**, 445 (2006).

[35] M. Nakatsutsumi, Y. Sentoku, A. Korzhimanov, S. N. Chen, S. Buffechoux, A. Kon, B. Atherton, P. Audebert, M. Geissel, L. Hurd *et al.*, *Self-Generated Surface Magnetic Fields Inhibit Laser-Driven Sheath Acceleration of High-Energy Protons*, Nat. Commun. **9**, 280 (2018).

[36] N. P. Dover, M. Nishiuchi, H. Sakaki, K. Kondo, M. A. Alkhimova, A. Y. Faenov, M. Hata, N. Iwata, H. Kiriyama, J. K. Koga *et al.*, *Effect of Small Focus on Electron Heating and Proton Acceleration in Ultrarelativistic Laser-Solid Interactions*, Phys. Rev. Lett. **124**, 084802 (2020).

[37] P. Mora, *Plasma Expansion into a Vacuum*, Phys. Rev. Lett. **90**, 185002 (2003).

[38] J. Fuchs, P. Antici, E. d'Humières, E. Lefebvre, M. Borghesi, E. Brambrink, C. A. Cecchetti, M. Kaluza, V. Malka, M. Manclossi *et al.*, *Laser-Driven Proton Scaling Laws and New Paths Towards Energy Increase*, Nat. Phys. **2**, 48 (2006).

[39] J. Schreiber, F. Bell, F. Grüner, U. Schramm, M. Geissler, M. Schnürer, S. Ter-Avetisyan, B. M. Hegelich, J. Cobble, E. Brambrink *et al.*, *Analytical Model for Ion Acceleration by High-Intensity Laser Pulses*, Phys. Rev. Lett. **97**, 045005 (2006).

[40] M. Chen, A. Pukhov, T. P. Yu, and Z.-M Sheng, *Enhanced Collimated GeV Monoenergetic Ion Acceleration from a Shaped Foil Target Irradiated by a Circularly Polarized Laser Pulse*, Phys. Rev. Lett. **103**, 024801 (2009).

[41] T.-P. Yu, A. Pukhov, G. Shvets, and M. Chen, *Stable Laser-Driven Proton Beam Acceleration from a Two-Ion-Species Ultrathin Foil*, Phys. Rev. Lett. **105**, 065002 (2010).

[42] T. Bartal, M. E. Foord, C. Bellei, M. H. Key, K. A. Flippo, S. A. Gaillard, D. T. Offermann, P. K. Patel, L. C. Jarrott, D. P. Higginson *et al.*, *Focusing of Short-Pulse High-Intensity Laser-Accelerated Proton Beams*, Nat. Phys. **8**, 139 (2012).

[43] X. F. Shen, B. Qiao, H. X. Chang, W. L. Zhang, H. Zhang, C. T. Zhou, and X. T. He, *Maintaining Stable Radiation Pressure Acceleration of Ion Beams via Cascaded Electron Replenishment*, New J. Phys. **19**, 033034 (2017).

[44] J. H. Bin, M. Yeung, Z. Gong, H. Y. Wang, C. Kreuzer, M. L. Zhou, M. J. V. Streeter, P. S. Foster, S. Cousens, B. Dromey *et al.*, *Enhanced Laser-Driven Ion Acceleration by Superponderomotive Electrons Generated from Near-Critical-Density Plasma*, Phys. Rev. Lett. **120**, 074801 (2018).

[45] D. B. Zou, D. Y. Yu, M. Y. Yu, T. W. Huang, A. Pukhov, H. B. Zhuo, C. T. Zhou, and S. C. Ruan, *Efficient Generation of* $\sim$*100 MeV Ions from Ultrashort* $\sim$$10^{21}$ *W cm*$^{-2}$ *Laser Pulse Interaction with a Waveguide Target*, Nucl. Fusion **59**, 066034 (2019).

[46] T. Toncian, M. Borghesi, J. Fuchs, E. d'Humieres, P. Antici, P. Audebert, E. Brambrink, C. A. Cecchetti, A. Pipahl, L. Romagnani, and O. Willi, *Ultrafast Laser-Driven Microlens to Focus and Energy-Select Mega-Electron Volt Protons*, Science **312**, 410 (2006).

[47] K. Markey, P. McKenna, C. M. Brenner, D. C. Carroll, M. M. Günther, K. Harres, S. Kar, K. Lancaster, F. Nürnberg, M. N. Quinn *et al.*, *Spectral Enhancement in the Double Pulse Regime of Laser Proton Acceleration*, Phys. Rev. Lett. **105**, 195008 (2010).

[48] W. P. Wang, B. F. Shen, H. Zhang, X. M. Lu, J. F. Li, S. H. Zhai, S. S. Li, X. L. Wang, R. J. Xu, C. Wang *et al.*, *Spectrum Tailoring of Low Charge-to-Mass Ion Beam by the Triple-Stage Acceleration Mechanism*, Phys. Plasmas **26**, 043102 (2019).

[49] S. Kar, H. Ahmed, R. Prasad, M. Cerchez, S. Brauckmann, B. Aurand, G. Cantono, P. Hadjisolomou, C. L. S. Lewis, A. Macchi *et al.*, *Guided Post-Acceleration of Laser-Driven Ions by a Miniature Modular Structure*, Nat. Commun. **7**, 10792 (2016).

[50] P. Hilz, T. M. Ostermayr, A. Huebl, V. Bagnoud, B. Borm, M. Bussmann, M. Gallei, J. Gebhard, D. Haffa, J. Hartmann *et al.*, *Isolated Proton Bunch Acceleration by a Petawatt Laser Pulse*, Nat. Commun. **9**, 423 (2018).

[51] A. V. Brantov, E. A. Govras, V. F. Kovalev, and V. Yu. Bychenkov, *Synchronized Ion Acceleration by Ultraintense Slow Light*, Phys. Rev. Lett. **116**, 085004 (2016).

[52] F. Mackenroth, A. Gonoskov, and M. Marklund, *Chirped-Standing-Wave Acceleration of Ions with Intense Lasers*, Phys. Rev. Lett. **117**, 104801 (2016).

[53] R. Matsui, Y. Fukuda, and Y. Kishimoto, *Quasimonoenergetic Proton Bunch Acceleration Driven by Hemispherically Converging Collisionless Shock in a Hydrogen Cluster Coupled with Relativistically Induced Transparency*, Phys. Rev. Lett. **122**, 014804 (2019).

[54] X. F. Shen, B. Qiao, H. Zhang, Y. Xie, S. Kar, M. Borghesi, M. Zepf, C. T. Zhou, S. P. Zhu, and X. T. He, *Electrostatic Capacitance-Type Acceleration of Ions with an Intense Few-Cycle Laser Pulse*, Appl. Phys. Lett. **114**, 144102 (2019).

[55] C. Riconda, M. Raynaud, T. Vialis, and M. Grech, *Simple Scalings for Various Regimes of Electron Acceleration in Surface Plasma Waves*, Phys. Plasmas **22**, 073103 (2015).

[56] A. Macchi, *Surface Plasmons in Superintense Laser-Solid Interactions*, Phys. Plasmas **25**, 031906 (2018).

[57] J. M. Pitarke, V. M. Silkin, E. V. Chulkov, and P. M. Echenique, *Theory of Surface Plasmons and Surface-Plasmon Polaritons*, Rep. Prog. Phys. **70**, 1 (2007).

[58] T. D. Arber, K. Bennett, C. S. Brady, A. Lawrence-Douglas, M. G. Ramsay, N. J. Sircombe, P. Gillies, R. G. Evans, H. Schmitz, A. R. Bell, and C. P. Ridgers, *Contemporary Particle-in-Cell Approach to Laser-Plasma Modelling*, Plasma Phys. Controlled Fusion **57**, 113001 (2015).

[59] A. Pukhov, *Particle-In-Cell Codes for Plasma-Based Particle Acceleration*, CERN Yellow Rep. **1**, 181 (2016).

[60] A. M. Perelomov, V. S. Popov, and M. V. Terent'ev, *Ionization of Atoms in an Alternating Electric Field*, Sov. Phys. JETP **23**, 924 (1966); *Ionization of Atoms in an Alternating Electric Field: II*, Sov. Phys. JETP **24**, 207 (1967).

[61] P. Mulser and D. Bauer, *High Power Laser-Matter Interaction* (Springer, Berlin, 2010).

[62] L. Fedeli, A. Sgattoni, G. Cantono, D. Garzella, F. Réau, I. Prencipe, M. Passoni, M. Raynaud, M. Květoň, J. Proska *et al.*, *Electron Acceleration by Relativistic Surface Plasmons in Laser-Grating Interaction*, Phys. Rev. Lett. **116**, 015001 (2016).

[63] G. Cantono, L. Fedeli, A. Sgattoni, A. Denoeud, L. Chopineau, F. Réau, T. Ceccotti, and A. Macchi, *Extreme Ultraviolet Beam Enhancement by Relativistic Surface Plasmons*, Phys. Rev. Lett. **120**, 264803 (2018).

[64] G. Cantono, A. Sgattoni, L. Fedeli, D. Garzella, F. Réau, C. Riconda, A. Macchi, and T. Ceccotti, *Extensive Study of Electron Acceleration by Relativistic Surface Plasmons*, Phys. Plasmas **25**, 031907 (2018).

[65] L. Chopineau, A. Leblanc, G. Blaclard, A. Denoeud, M. Thévenet, J-L. Vay, G. Bonnaud, P. Martin, H. Vincenti, and F. Quéré, *Identification of Coupling Mechanisms between Ultraintense Laser Light and Dense Plasmas*, Phys. Rev. X **9**, 011050 (2019).

[66] O. Svelto, *Principles of Lasers* (Springer, New York, 2010).

[67] A. Pukhov, Z.-M. Sheng, and J. Meyer-ter-Vehn, *Particle Acceleration in Relativistic Laser Channels*, Phys. Plasmas **6**, 2847 (1999).

[68] A. Pukhov and J. Meyer-ter-Vehn, *Laser Wake Field Acceleration: The Highly Non-linear Broken-Wave Regime*, Appl. Phys. B **74**, 355 (2002).

[69] S. C. Wilks, W. L. Kruer, M. Tabak, and A. B. Langdon, *Absorption of Ultra-Intense Laser Pulses*, Phys. Rev. Lett. **69**, 1383 (1992).

[70] J. E. Crow, P. L. Auer, and J. E. Allen, *The Expansion of a Plasma into a Vacuum*, J. Plasma Phys. **14**, 65 (1975).

[71] X. Q. Yan, C. Lin, Z.-M. Sheng, Z. Y. Guo, B. C. Liu, Y. R. Lu, J. X. Fang, and J. E. Chen, *Generating High-Current Monoenergetic Proton Beams by a Circularly Polarized Laser Pulse in the Phase-Stable Acceleration Regime*, Phys. Rev. Lett. **100**, 135003 (2008).

[72] A. Macchi, S. Veghini, and F. Pegoraro, *"Light Sail" Acceleration Reexamined*, Phys. Rev. Lett. **103**, 085003 (2009).

[73] D. Haberberger, S. Tochitsky, F. Fiuza, C. Gong, R. A. Fonseca, L. O. Silva, W. B. Mori, and C. Joshi, *Collisionless Shocks in Laser-Produced Plasma Generate Monoenergetic High-Energy Proton Beams*, Nat. Phys. **8**, 95 (2012).

[74] See Supplemental Material at http://link.aps.org/supplemental/10.1103/PhysRevX.11.041002 for details. It mainly includes the discussions about the robustness of the scheme to the variation of plate dimensions (width and thickness), incidence angle, plasma density, and existence of preplasmas. In addition, a schematic of a possible experimental setup is shown.

[75] K. Nakamura, H.-S. Mao, A. J. Gonsalves, D. E. Mittelberger, J. Daniels, A. Magana, C. Toth, and W. P. Leemans, *Diagnostics, Control and Performance Parameters for the BELLA High Repetition Rate Petawatt Class Laser*, IEEE J. Quantum Electron. **53**, 1200121 (2017).

[76] L. Obst, S. Göde, M. Rehwald, F.-E. Brack, J. Branco, S. Bock, M. Bussmann, T. E. Cowan, Ch. B. Curry, F. Fiuza *et al.*, *Efficient Laser-Driven Proton Acceleration from Cylindrical and Planar Cryogenic Hydrogen Jets*, Sci. Rep. **7**, 10248 (2017).

[77] J. M. Cole, K. T. Behm, E. Gerstmayr, T. G. Blackburn, J. C. Wood, C. D. Baird, M. J. Duff, C. Harvey, A. Ilderton, A. S. Joglekar *et al.*, *Experimental Evidence of Radiation Reaction in the Collision of a High-Intensity Laser Pulse with a Laser-Wakefield Accelerated Electron Beam*, Phys. Rev. X **8**, 011020 (2018).

[78] K. Poder, M. Tamburini, G. Sarri, A. Di Piazza, S. Kuschel, C. D. Baird, K. Behm, S. Bohlen, J. M. Cole, D. J. Corvan *et al.*, *Experimental Signatures of the Quantum Nature of Radiation Reaction in the Field of an Ultraintense Laser*, Phys. Rev. X **8**, 031004 (2018).

[79] ELI Beamlines Strategic Development Plan, 2018–2024, https://www.eli-beams.eu/wp-content/uploads/2018/08/ELI_BL_Strategic-development-plan_2018-2024.pdf.

[80] D. A. Serebryakov, E. N. Nerush, and I. Yu. Kostyukov, *Near-Surface Electron Acceleration During Intense Laser Solid Interaction in the Grazing Incidence Regime*, Phys. Plasmas **24**, 123115 (2017).

[81] M. Roth, A. Blazevic, M. Geissel, T. Schlegel, T. E. Cowan, M. Allen, J.-C. Gauthier, P. Audebert, J. Fuchs, J. Meyer-ter-Vehn *et al.*, *Energetic Ions Generated by Laser Pulses: A Detailed Study on Target Properties*, Phys. Rev. Accel. Beams **5**, 061301 (2002).

[82] I. Prencipe, J. Fuchs, S. Pascarelli, D. W. Schumacher, R. B. Stephens, N. B. Alexander, R. Briggs, M. Büscher, M. O. Cernaianu, A. Choukourov *et al.*, *Targets for High Repetition Rate Laser Facilities: Needs, Challenges and Perspectives*, High Power Laser Sci. Eng. **5**, e17 (2017).

[83] T. Chagovets, S. Stancek, L. Giuffrida, A. Velyhan, M. Tryus, F. Grepl, V. Istokskaia, V. Kantarelou, T. Wiste, J. Carlos, H. Martin *et al.*, *Automation of Target Delivery and Diagnostic Systems for High Repetition Rate Laser-Plasma Acceleration*, Appl. Sci. **11**, 1680 (2021).

[84] L. A. Gizzi, G. Cristoforetti, F. Baffigi, F. Brandi, G. D'Arrigo, A. Fazzi, L. Fulgentini, D. Giove, P. Koester, L. Labate *et al.*, *Intense Proton Acceleration in Ultra-relativistic Interaction with Nanochannels*, Phys. Rev. Research **2**, 033451 (2020).

[85] G. Cristoforetti, F. Baffigi, F. Brandi, G. D'Arrigo, A. Fazzi, L. Fulgentini, D. Giove, P. Koester, L. Labate, G. Maero *et al.*, *Laser-Driven Proton Acceleration via Excitation of Surface Plasmon Polaritons into* TiO_2 *Nanotube Array Targets*, Plasma Phys. Controlled Fusion **62**, 114001 (2020).

[86] V. Kaymak, A. Pukhov, V. N. Shlyaptsev, and J. J. Rocca, *Nanoscale Ultradense Z-Pinch Formation from Laser-Irradiated Nanowire Arrays*, Phys. Rev. Lett. **117**, 035004 (2016).

[87] L. Yi, B. Shen, A. Pukhov, and T. Fülöp, *Relativistic Magnetic Reconnection Driven by a Laser Interacting with a Micro-Scale Plasma Slab*, Nat. Commun. **9**, 1601 (2018).